



# Pharmacological properties of SAK3, a novel T-type voltage-gated $\text{Ca}^{2+}$ channel enhancer



Yasushi Yabuki <sup>a</sup>, Kazuya Matsuo <sup>a</sup>, Hisanao Izumi <sup>a</sup>, Hidaka Haga <sup>a</sup>, Takashi Yoshida <sup>b</sup>, Minoru Wakamori <sup>b</sup>, Akikazu Kakei <sup>c</sup>, Kenji Sakimura <sup>d</sup>, Takaichi Fukuda <sup>e</sup>, Kohji Fukunaga <sup>a,\*</sup>

<sup>a</sup> Department of Pharmacology, Graduate School of Pharmaceutical Sciences, Tohoku University, Sendai, Japan

<sup>b</sup> Department of Oral Biology, Graduate School of Dentistry, Tohoku University, Sendai, Japan

<sup>c</sup> Department of Chemistry and Material Engineering, Faculty of Engineering, Shinshu University, Nagano, Japan

<sup>d</sup> Department of Cellular Neurobiology, Brain Research Institute, Niigata University, Niigata, Japan

<sup>e</sup> Department of Anatomy and Neurobiology, Graduate School of Medical Sciences, Kumamoto University, Kumamoto, Japan

## ARTICLE INFO

### Article history:

Received 16 July 2016

Received in revised form

27 December 2016

Accepted 12 January 2017

Available online 16 January 2017

### Keywords:

T-type voltage-gated  $\text{Ca}^{2+}$  channel

Acetylcholine

Memory

Cognitive function

Spiroimidazopyridine

## ABSTRACT

T-type voltage-gated  $\text{Ca}^{2+}$  channels (T-VGCCs) function in the pathophysiology of epilepsy, pain and sleep. However, their role in cognitive function remains unclear. We previously reported that the cognitive enhancer ST101, which stimulates T-VGCCs in rat cortical slices, was a potential Alzheimer's disease therapeutic. Here, we introduce a more potent T-VGCC enhancer, SAK3 (ethyl 8'-methyl-2',4'-dioxo-2-(piperidin-1-yl)-2'H-spiro[cyclopentane-1,3'-imidazo [1,2-a]pyridin]-2-ene-3-carboxylate), and characterize its pharmacological properties in brain. Based on whole cell patch-clamp analysis, SAK3 (0.01–10 nM) significantly enhanced Cav3.1 currents in neuro2A cells ectopically expressing Cav3.1. SAK3 (0.1–10 nM) also enhanced Cav3.3 but not Cav3.2 currents in the transfected cells. Notably, Cav3.1 and Cav3.3 T-VGCCs were localized in cholinergic nerve systems in hippocampus and in the medial septum. Indeed, acute oral administration of SAK3 (0.5 mg/kg, p.o.), but not ST101 (0.5 mg/kg, p.o.) significantly enhanced acetylcholine (ACh) release in the hippocampal CA1 region of naïve mice. Moreover, acute SAK3 (0.5 mg/kg, p.o.) administration significantly enhanced hippocampal ACh levels in olfactory-bulbectomized (OBX) mice, rescuing impaired memory-related behaviors. Treatment of OBX mice with the T-VGCC-specific blocker NNC 55-0396 (12.5 mg/kg, i.p.) antagonized both enhanced ACh release and memory improvements elicited by SAK3 administration. We also observed that SAK3-induced ACh releases were significantly blocked in the hippocampus from Cav3.1 knockout (KO) mice. These findings suggest overall that T-VGCCs play a key role in cognition by enhancing hippocampal ACh release and that the cognitive enhancer SAK3 could be a candidate therapeutic in Alzheimer's disease.

© 2017 Elsevier Ltd. All rights reserved.

## 1. Introduction

Low-threshold T-type voltage gated  $\text{Ca}^{2+}$  channels (T-VGCCs) show unique electrophysiological features with the fast

inactivation and slow deactivation kinetics (Huguenard, 1996; Perez-Reyes, 2003).  $\text{Ca}^{2+}$  influx through T-VGCCs evokes low-threshold  $\text{Ca}^{2+}$  spikes and then triggers burst firing mediated by  $\text{Na}^{+}$  channels in many neurons (Huguenard, 1996; Perez-Reyes,

*Abbreviations:* ACh, acetylcholine; AChE, acetylcholine esterase; ANOVA, analysis of variance; CaMKII,  $\text{Ca}^{2+}$ /calmodulin-dependent protein kinase II; ChAT, choline acetyltransferase; DMEM, Dulbecco's minimal essential medium; ECD, electrochemical detector; FBS, fetal bovine serum; GFP, green fluorescent protein; HPLC, high-performance liquid chromatography; I-V, current and voltage; KO, knockout; LTP, long-term potentiation; mAChR, muscarinic ACh receptor; nAChR, nicotinic ACh receptor; NMDG, N-methyl-D-glucamine; OBX, olfactory-bulbectomized; PBS, phosphate-buffered saline; PKA, protein kinase A; PKC, protein kinase C; SAK, spiroimidazopyridine derivative; SAK3, ethyl-8'-methyl-2',4'-dioxo-2-(piperidin-1-yl)-2'H-spiro[cyclopentane-1,3'-imidazo[1,2-a]pyridin]-2-ene-3-carboxylate; ST101, piro[imidazo[1,2-a]pyridine-3,2-indan]-2(3H)-one; 3xTg, triple-transgenic; TTX, tetrodotoxin; T-VGCC, T-type voltage-gated  $\text{Ca}^{2+}$  channel; WT, wild type.

\* Corresponding author. Department of Pharmacology, Graduate School of Pharmaceutical Sciences, Tohoku University, Aramaki-Aoba Aoba-ku, Sendai 980-8578, Japan.

E-mail address: [kfukunaga@m.tohoku.ac.jp](mailto:kfukunaga@m.tohoku.ac.jp) (K. Fukunaga).

2003). All three T-VGCC subtypes encoded by *CACNA1G* (Cav3.1), *CACNA1H* (Cav3.2) and *CACNA1I* (Cav3.3) genes are expressed in brain and function in physiological and pathological events, including sleep, epilepsy and pain (McCormick and Bal, 1997; Talley et al., 1999; Crunelli et al., 2006; Zamponi et al., 2010; François et al., 2014).

Recent studies suggest that T-VGCCs function in maintenance of synaptic plasticity in hippocampus and cortex. For example, blocking T-VGCC with 50  $\mu$ M  $\text{Ni}^{2+}$  disrupts induction of long-term depression in layer 2/3 pyramidal neurons of rat somatosensory cortex (Nevian and Sakmann, 2006) and abolishes low-threshold spikes that boosts fast  $\text{Na}^+$  action potentials in newly generated granule cells in adult rat hippocampus (Schmidt-Hieber et al., 2004). Moreover, phospholipase C $\beta$ 4 knockout mice exhibit impaired fear extinction learning accompanied by elevated T-VGCC currents in the mediodorsal thalamic nucleus, and intramediodorsal thalamic infusion of the T-VGCC inhibitor mibefradil rescues abnormal extinction behavior (Lee et al., 2011). Thus, T-VGCCs are clearly important for normal memory and cognitive function.

We previously developed a novel cognitive enhancer ST101 (ZSET1446: spiro[imidazo[1,2-a]pyridine-3,2-indan]-2(3H)-one), which enhances Cav3.1 T-VGCC currents in Cav3.1-transfected neuro2A cells (Moriguchi et al., 2012). ST101 also enhances activity of  $\text{Ca}^{2+}$ /calmodulin-dependent protein kinase II (CaMKII), promoting long-term potentiation (LTP) in rat somatosensory cortical slices via T-VGCC stimulation (Moriguchi et al., 2012). In addition, ST101 treatment significantly improves impaired memory-related behaviors observed in olfactory bulbectomized (OBX) mice (Han et al., 2008; Yamamoto et al., 2013). Interestingly, acute intraperitoneal administration of ST101 (1.0 mg/kg, i.p.) accelerates hippocampal acetylcholine (ACh) release, an effect blocked by mibefradil (Yamamoto et al., 2013). Green et al. (2011) reported that impaired spatial memory observed in triple-transgenic (3xTg) Alzheimer's model mice was restored by chronic ST101 administration. These observations suggest that T-VGCC stimulation could be an attractive strategy in developing novel Alzheimer's disease (AD) therapeutics. In fact, combined administration of ST101 with the cholinesterase inhibitor donepezil maintains memory performance in AD patients, although treatment with ST101 alone showed little benefit for patients in a phase II clinical trial in the USA (Gauthier et al., 2015).

In the present study, we report development of SAK3 (ethyl-8'-methyl-2',4'-dioxo-2-(piperidin-1-yl)-2'H-spiro[cyclopentane-1,3'-imidazo [1,2-a]pyridin]-2-ene-3-carboxylate), a more effective T-VGCC enhancer, and characterize its pharmacological properties in potentially enhancing cognition. We demonstrate that both Cav3.1 and 3.3 T-VGCCs are SAK3 targets and that both channels are expressed in the hippocampal and septum cholinergic neurons. Furthermore, acute SAK3 but not ST101 administration promoted ACh release in the hippocampus via T-VGCC enhancement in mouse brain.

## 2. Materials and methods

### 2.1. Animals and olfactectomy

Eight-week-old male ddY mice were purchased from Clea Japan, Inc. (Tokyo, Japan). Cav3.1 KO mice were generated by Dr. Kenji Sakimura (Handforth et al., 2010). Animals were bred under conditions of  $23 \pm 2$  °C, humidity  $55 \pm 5\%$ , a light and dark cycle (light from 9am to 9pm) and unlimited access to food and water. All animal experiments were approved by the Committee on Animal Experiments at Tohoku University. Efforts were made to minimize animal stress and the number of mice used.

After a habituation period of 1 week, OBX mice were prepared according to previous reports (Han et al., 2008; Yamamoto et al., 2013). In brief, mice were anesthetized and their head immobilized by a stereotaxic apparatus (David Kopf Instruments, Tujunga, CA, U.S.A.). A small burr hole was drilled on both sides of the olfactory bulbs, which were then removed using a suction pump. Holes were filled with hemostatic sponges to prevent hemorrhagia. Two weeks later, mice were subjected to behavioral analyses.

### 2.2. Drug administration

SAK3 was synthesized and supplied from Dr. Akikazu Kakei (Abe et al., 2010; Fig. 1C). ST101 and SAK3 (Fig. 1A) were dissolved in distilled water. Animals were orally administered either ST101 (0.5 mg/kg, p.o.) or SAK3 (0.1, 0.5 and 1.0 mg/kg, p.o.). Thirty minutes prior to oral administration of either ST101 (0.5 mg/kg, p.o.) or SAK3 (0.5 mg/kg, p.o.), some animals were treated with or without the T-VGCC-specific blocker NNC 55-0396 (12.5 mg/kg, i.p.; Sigma-Aldrich, St-Louis, MO, USA). Sham-operated mice were administered the same volume of distilled water, ST101 (0.5 mg/kg, p.o.) or SAK3 (0.5 mg/kg, p.o.).

We designed four experimental groups of different animals to minimize stress effects. (1) Group I was used to evaluate memory-related behaviors 2 weeks after olfactory bulb removal ( $n = 6$  per group). (2) Group II was subjected to *in vivo* microdialysis as naïve mice ( $n = 5$  per group). (3) Group III was evaluated for ACh content using high-performance liquid chromatography (HPLC) ( $n = 5$ – $7$  per group). (4) Group IV underwent immunohistochemical analysis and western blotting procedures ( $n = 4$ – $6$  per group).

### 2.3. Behavioral analyses

#### 2.3.1. Y-maze task

Spatial memory was evaluated using a Y-maze task (Yabuki et al., 2014, 2015). Briefly, a mouse was placed on the end of one arm and allowed to move freely in the maze during 8-min. Alternation behavior was defined as entries into all three arms on consecutive choices. Animals were administered with ST101 (0.5 mg/kg, p.o.) or SAK3 (0.1, 0.5 or 1.0 mg/kg, p.o.) 30 min before Y-maze task. The maximum number of alternations was defined as the total number of arms entered minus two, and the percentage of alternations was calculated as actual alternations/maximum alternations  $\times$  100.

#### 2.3.2. Step-through passive avoidance task

This task was evaluated as described (Yabuki et al., 2014, 2015). The apparatus consisted of light and dark compartments with stainless steel rods connected with an electronic stimulator (Nihon Kohden, Tokyo, Japan). When the mouse entered the dark compartment, it received an electric shock (0.3 mA for 2 s) from the grid floor and was removed from the apparatus 30 s later on training trials (fear acquisition). Twenty-four hours after this fear acquisition session, mice were placed in the light compartment and step-through latency was recorded over a period of 300s an indicator of retention level (test session). Animals were administered with ST101 (0.5 mg/kg, p.o.) or SAK3 (0.1, 0.5 or 1.0 mg/kg, p.o.) 30 min before both acquisition and test session.

#### 2.3.3. Novel object recognition task

This task was performed as described (Yabuki et al., 2014, 2015). In the trial session, two similar objects were placed symmetrically in the center of the open field box for 10 min. Twenty four hours later, one object was replaced with a novel object and exploratory behavior was monitored again for 5 min (test session). A discrimination index was evaluated by comparing the difference between

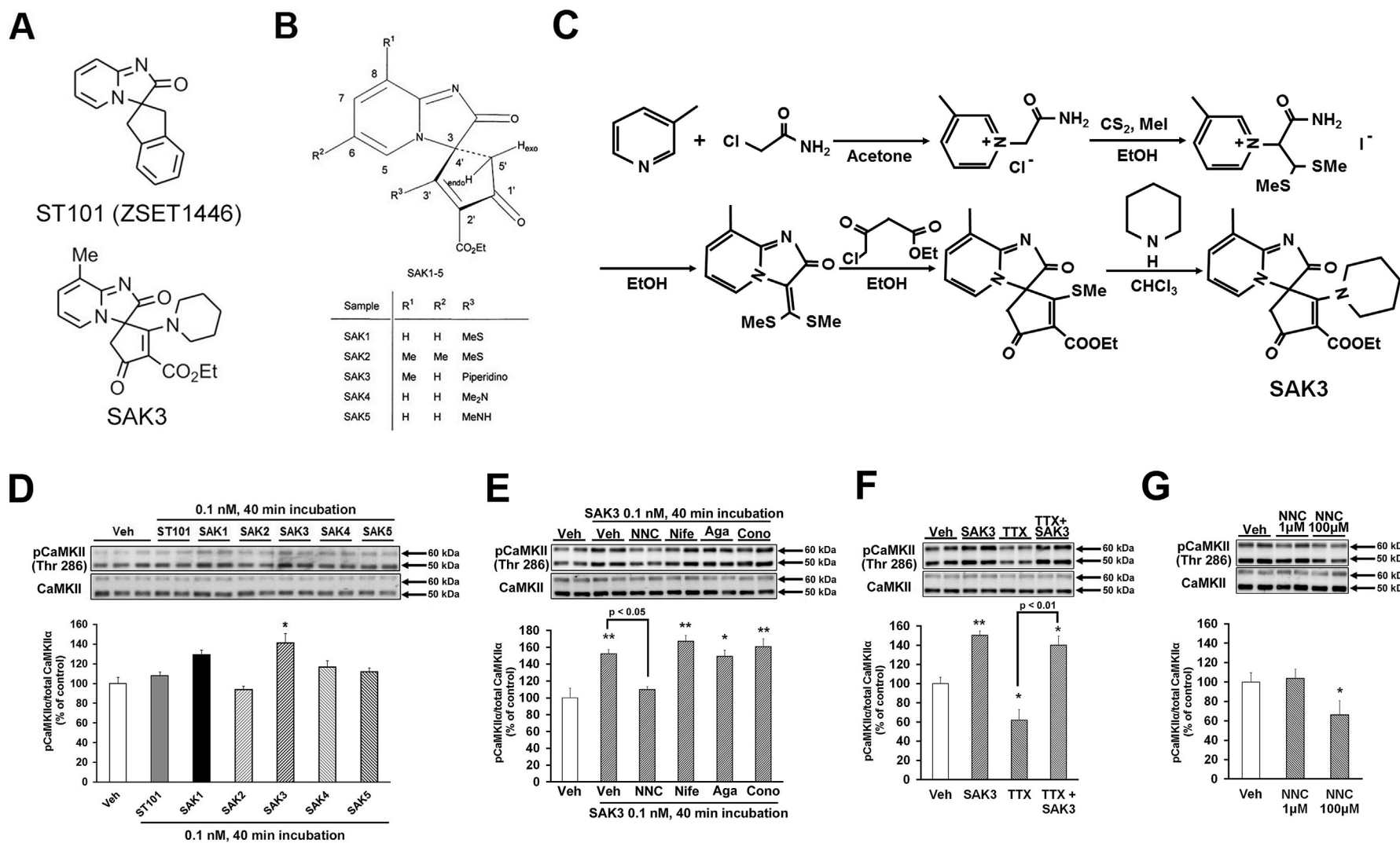


**Fig. 1.** Compound structures and the effect of SAKs on hippocampal CaMKII activity. (A) Shown are chemical structures of ST101 (up) and SAK3 (down). (B) Structures of SAK1-5. (C) Synthetic scheme of SAK3. (D, E, F, G) Representative images of western blots probed with antibodies against autophosphorylated CaMKII (Thr 286) and CaMKII in the hippocampal CA1 region (upper). (D) The hippocampal slices were incubated in ACSF buffer with respective SAKs (0.1 nM) for 40 min [Thr 286: vehicle incubation (n = 6), other groups (n = 4 per group)]. (E) T-VGCC blocker: NNC 55-0396 1  $\mu$ M, L-VGCC blocker: nifedipine 10  $\mu$ M, P/Q-VGCC blocker:  $\omega$ -Agatoxin TK 30 nM or N-VGCC blocker:  $\omega$ -Conotoxin GVIA 1  $\mu$ M was incubated 30 min before SAK3 (0.1 nM) application in the hippocampal slice (n = 6 per group). (F) TTX (100 nM) did not prevent CaMKII activation following SAK3 (0.1 nM) application (n = 6 per group). (G) NNC 55-0396 (1  $\mu$ M) did not inhibit basal CaMKII activity (n = 4 per group). Error bars represent SEM. \*p < 0.05 vs. vehicle incubation, \*\*p < 0.01 vs. vehicle incubation; Aga:  $\omega$ -Agatoxin TK application, Cono:  $\omega$ -Conotoxin GVIA application, Nife: nifedipine application, NNC: NNC 55-0396 application, Veh: vehicle incubation, Me: methyl.

exploratory contacts of novel or familiar objects and the total number of contacts, adjusting for differences in total exploration contacts. Animals were administered with ST101 (0.5 mg/kg, p.o.) or SAK3 (0.1, 0.5 or 1.0 mg/kg, p.o.) 30 min before both trial and test session.

#### 2.4. Cell culture and transfection

Neuro2A mouse neuroblastoma cells were obtained from the Human Science Research Resources Bank (Osaka, Japan). Cells were grown in Dulbecco's minimal essential medium (DMEM, Invitrogen, Carlsbad, CA, USA) including 10% heat-inactivated fetal bovine serum (FBS) and penicillin/streptomycin (100 units/100 µg/ml) in a 5% CO<sub>2</sub> incubator at 37 °C. Cells were transfected with DNA mixtures containing respective pcDNA plasmids (2.0 µg/mL) encoding human-Cav3.1, Cav3.2 or Cav3.3 plus 0.1% green fluorescent protein (GFP) plasmid as described (Moriguchi et al., 2012). Forty-eight hours later, cells were re-plated in 35 mm dishes for electrophysiological recording to be performed the following day.

#### 2.5. Whole-cell patch-clamp recording

Recording was performed as described (Takahashi and Akaike, 1991; Wakamori et al., 1993; Chemin et al., 2007). The external solution contained 143 mM NaCl, 5 mM KCl, 2 mM CaCl<sub>2</sub>, 1 mM MgCl<sub>2</sub>, 10 mM glucose and 10 mM HEPES (Tyrode's solution; pH adjusted to 7.4 with NaOH, osmotic pressure 300–330 mos<sub>M</sub>). Glass pipettes were filled with internal solution containing 100 mM *N*-methyl-D-glucamine (NMDG)-fluoride, 45 mM TEA-Cl, 5 mM EGTA and 5 mM HEPES (Takahashi and Akaike, 1991; pH adjusted to 7.4 with NMDG, osmotic pressure 290–320 mos<sub>M</sub>). The resistance of electrodes filled with internal solution was 3.0–4.5 MΩ. For recording T-VGCC currents, tetrodotoxin (TTX; 100 nM) added to the external solution to block voltage-gated sodium channel currents. Rapid drug application was performed using the Y-tube method (Wakamori et al., 1993). Each Cav3 current was recorded at room temperature using an EPC10 single patch clamp amplifier and acquisition system (HEKA, Lambrecht, Germany), filtered at 3 kHz, and sampled at 10 kHz. Membrane potentials were clamped at -110 mV, unless otherwise stated, to measure current and voltage (*I*-*V*) relationships and peak currents. T-VGCC currents were normalized to membrane capacitance. To evaluate biophysical properties, steady-state activation (activation curve) and inactivation (inactivation curve) were analyzed. For the activation curve, tail currents were evoked by repolarization to -80 mV after 5-ms test pulses from -80 to 20 mV with 5 mV increments. For the inactivation curve, currents were elicited by 10 ms test pulses to -40 mV after a 10 ms repolarization to -130 mV following 2 s holding potential displacement (conditioning pulse) from -130 to -50 mV with 10 mV increments. Current amplitudes induced by test pulses were normalized to those evoked by the test pulse after 2 s holding potential displacement to -130 mV. Mean values were plotted and fitted to the Boltzmann equation as described (Kato et al., 2002).

#### 2.6. Western blotting analysis

We used western blotting to measure CaMKII activities in a screen for highly activated SAKs and SAK3 targets as described (Yabuki et al., 2014, 2015; Moriguchi et al., 2012). In brief, hippocampal slices were incubated in ACSF buffer with respective SAKs (0.1 nM) for 40 min. Each VGCCs inhibitor and TTX (100 nM) were incubated 30 min before SAK3 (0.1 nM) incubation. Specific VGCC blockers were used as T-VGCC blocker: NNC 55-0396 (1 or 100 µM, L-VGCC blocker: nifedipine (10 µM; Sigma-Aldrich), P/Q-VGCC blocker: ω-Agatoxin TK (30 nM; PEPTIDE INSTITUTE, INC., Osaka,

Japan) and N-VGCC blocker: ω-Conotoxin GVIA (1 µM; PEPTIDE INSTITUTE, INC). The CA1 region was then dissected, frozen in liquid nitrogen and stored at -80 °C until analysis. Tissues were homogenized and protein concentration was determined using Bradford's assay. Equal amounts of protein were loaded onto SDS-polyacrylamide gels and transferred to an Immobilon polyvinylidene difluoride membranes, which were incubated with anti-phospho-CaMKII (1:5000; Fukunaga et al., 1988) and anti-CaMKII (1:5000; Fukunaga et al., 1988) overnight at 4 °C. Blots were developed using an ECL immunoblotting detection system (Amersham Biosciences, NJ, USA) and signals were detected using Image Gauge version 3.41 (Fuji Film, Tokyo, Japan).

#### 2.7. Immunohistochemistry

Immunohistochemistry was performed as described (Yabuki and Fukunaga, 2013; Miyamoto and Fukuda, 2015). Naïve mice were perfused with ice-cold phosphate-buffered saline (PBS, pH 7.4) and then with 4% paraformaldehyde (Sigma-Aldrich). After removal and postfixation of the brain, tissue was sliced into 50 µm-thick coronal sections using a vibratome (Dosaka EM Co. Ltd., Kyoto, Japan). Briefly, brain slices were incubated with 1% bovine serum albumin and 0.3% Triton-X in PBS (blocking solution) overnight and then incubated with primary antibody diluted in blocking solution for 7 days at 4 °C. Antibodies included guinea pig polyclonal anti-Cav3.1 (1:200, Frontier Institute Co., Ltd., Ishikari, Hokkaido, Japan), rabbit polyclonal anti-Cav3.3 (1:200, Sigma-Aldrich) and/or goat polyclonal anti-choline acetyltransferase (ChAT) antibodies (1:200; Millipore, Billerica, MA, USA). After PBS washing, sections were incubated with Alexa 488 anti-guinea pig IgG (1:500; Jackson ImmunoResearch, West Grove, PA, USA) or Alexa 488 anti-rabbit IgG (1:500; Jackson ImmunoResearch), and with Alexa 594 anti-goat IgG (1:500; Jackson ImmunoResearch) overnight. After several PBS washes, sections were mounted in Vectashield (Vector Laboratories, Inc. Burlingame, CA, USA). Immunofluorescent images were analyzed using a confocal laser scanning microscope (LSM700, Zeiss, Thornwood, NY, USA). The position of the dorsal hippocampus and medial septum was identified using a mouse brain atlas (Paxinos and Franklin, 2001).

#### 2.8. Measurement of ACh release by *in vivo* microdialysis

Stereotaxic surgery for microdialysis was performed in mice as described (Yamamoto et al., 2013; Yabuki et al., 2014). After anesthesia, a small hole was drilled in order to implant a microdialysis probe in the brain. A guide cannula (AG-4; Eicom, Kyoto, Japan) was inserted into the dorsal hippocampal CA1 region [2.9 mm posterior and 3.3 mm lateral to the bregma and 1.4 mm below the brain surface, according to Paxinos and Franklin (2001)], and the skull was covered with dental cement. The microdialysis probe (A-I-4-02; Eicom) was induced through the guide cannula into the hippocampal CA1 region. After recovery, Ringer's solution was perfused at 1.25 µl/min using a microsyringe pump (ESP-64; Eicom) under free moving conditions. Perfused dialysates were collected every 20 min in the sample loop of an auto-injector (EAS-20; Eicom) connected to an HPLC-Electrochemical detector (ECD) system (HTEC-500; Eicom). When basal ACh levels reached steady state, mice were administered ST101 (0.5 mg/kg p.o.) or SAK3 (0.5 mg/kg p.o.). The T-VGCC-specific blocker NNC 55-0396 (1 µM; Sigma-Aldrich) in Ringer's solution was administered to hippocampal CA1 through a microdialysis probe 40 min before SAK3 administration. ACh release was assessed as a percentage of basal levels (Fig. 4A). ACh levels were calculated 0–60 min after drug treatment and compared to those seen in vehicle-treated animals at comparable time-points (Fig. 4B).

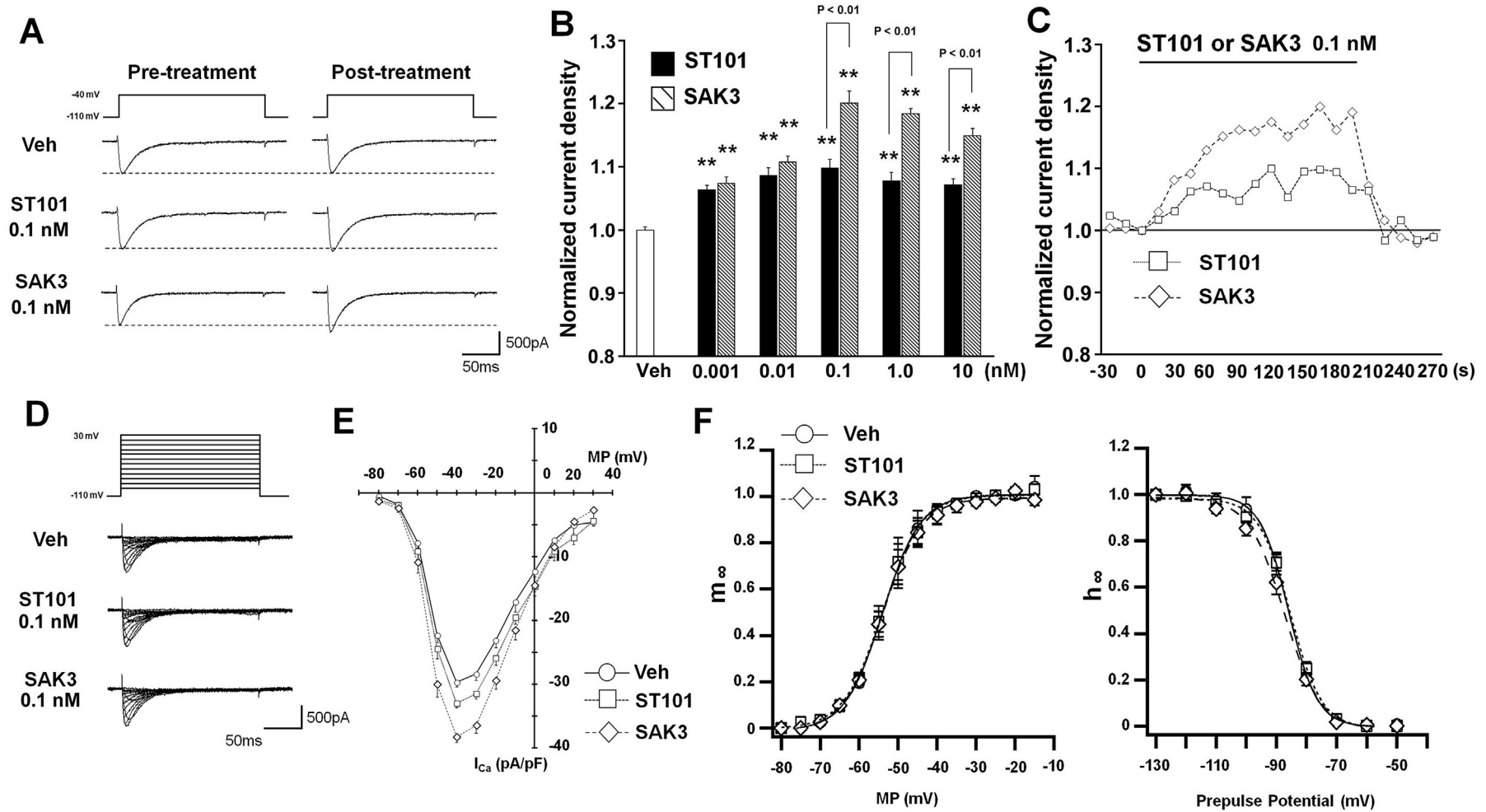


**Fig. 2.** The effect of ST101 and SAK3 on T-VGCC currents in neuro2A cells transfected with Cav3.1 expression vectors. (A) Representative traces of Cav3.1 peak current following treatment of cells with vehicle, ST101 (0.1 nM) or SAK3 (0.1 nM). (B) Dose responses following ST101 or SAK3 application were analyzed from 0.001 to 10 nM ( $n = 10-14$  per group). (C) Time courses following ST101 (0.1 nM) or SAK3 (0.1 nM) application. (D) Representative traces of Cav3.1 voltage-dependent currents following treatment of cells with vehicle, ST101 (0.1 nM) or SAK3 (0.1 nM). (E)  $I-V$  relationships following vehicle, ST101 (0.1 nM) or SAK3 (0.1 nM) application ( $n = 4-5$  per group). (F) Steady-state activation (left:  $n = 4$  per group) and inactivation (right:  $n = 5$  per group) curves were fitted to the Boltzmann equation. Error bars represent SEM. \*\* $p < 0.01$  vs. vehicle application; Veh: vehicle application.

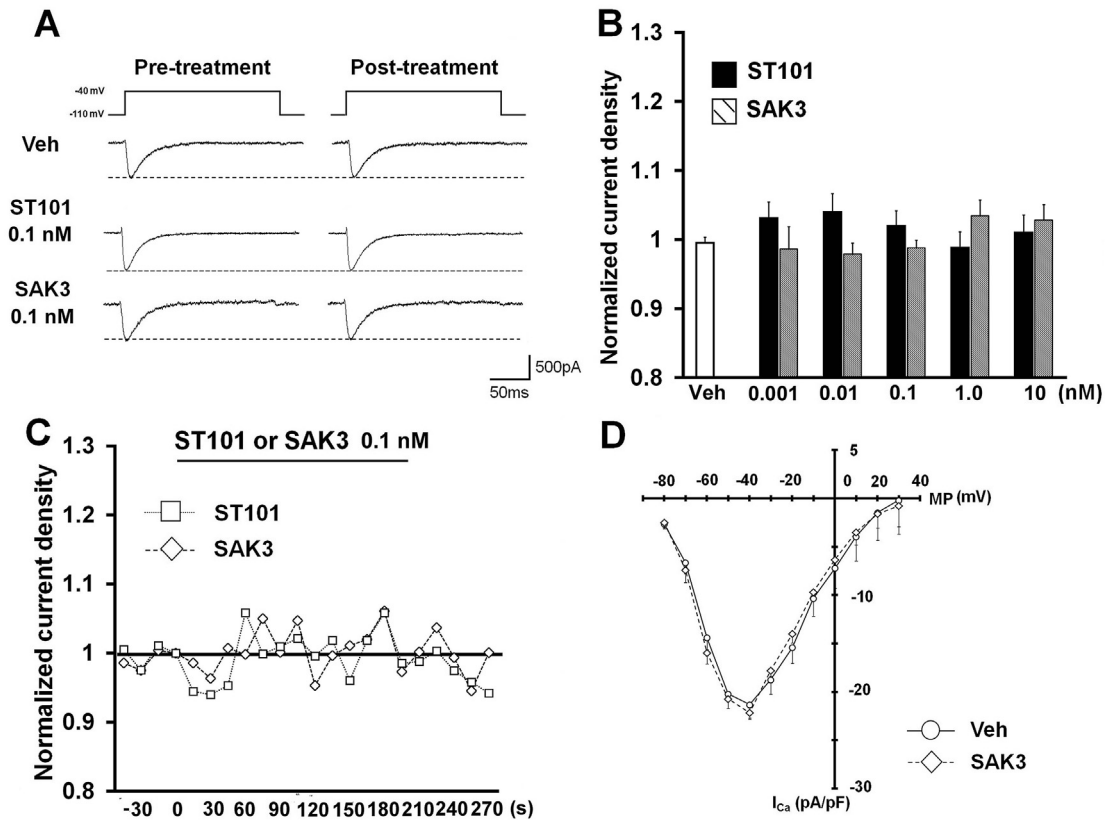


**Fig. 3.** Both ST101 and SAK3 application do not affect Cav3.2 currents. (A) Representative traces of Cav3.2 peak current following vehicle, ST101 (0.1 nM) or SAK3 (0.1 nM) application. (B) Dose responses following ST101 or SAK3 application were analyzed from 0.001 to 10 nM ( $n = 5$  per group). (C) Time course of Cav3.2 current as ST101 (0.1 nM) or SAK3 (0.1 nM) is applied. (D) SAK3 failed to enhance Cav3.2 currents ( $n = 4$  per group). Error bars represent SEM. Veh: vehicle application.

### 2.9. Measurement of ACh content in hippocampal CA1

To prevent ACh degradation by acetylcholine esterase (AChE), mouse hippocampal tissues were collected as described (Bertrand et al., 1994). In brief, after decapitation, mouse brains were rapidly removed and irradiated for 3.0 s in a microwave oven (power output: 750 W) to inactivate AChE. Tissues were then dissected, frozen in liquid nitrogen and stored at  $-80^{\circ}\text{C}$  until assayed. ACh content was evaluated according to the manufacturer's protocol from Eicom Ltd. Frozen tissues were weighed and homogenized in buffer with 0.1 M  $\text{HClO}_4$  and 100  $\mu\text{M}$  EDTA-2Na containing 10 nmol ethyhomocholine as an internal standard. Homogenates were centrifuged at  $20,000\times g$  for 15 min at  $4^{\circ}\text{C}$ . ACh content in supernatants were quantified by HPLC with ECD (HTEC-500; Eicom) using a reverse phase ion pair chromatography column (Eicompak AC-GEL; Eicom), and data were expressed as fmol/mg tissue weight.

### 2.10. Statistical analysis

Data are shown as means  $\pm$  standard error of the mean (SEM). Significant differences were determined using Student's *t*-test for two-group comparison or a one-way analysis of variance (ANOVA) for multi-group comparisons followed by Dunnett's test.  $p < 0.05$  represented a statistically significant difference.

## 3. Results

### 3.1. SAK3 potentiates Cav3.1 currents more robustly than ST101

We began by evaluating five novel ST101 derivatives (SAK 1-5)

(Fig. 1B) for their capacity to enhance CaMKII autophosphorylation in acute hippocampal slices. Among them, SAK3 (0.1 nM) significantly increased levels of autophosphorylated CaMKII in the CA1 region relative to vehicle only after a 40 min incubation ( $141.3 \pm 9.8$ ,  $p < 0.01$  vs. vehicle; Fig. 1D). Then, we confirmed whether SAK3 (0.1 nM) promotes CaMKII autophosphorylation levels via enhancing T-VGCC. T-VGCC specific blocker NNC 55-0396 (1  $\mu\text{M}$ ) but not another VGCC blockers significantly inhibited the elevated CaMKII autophosphorylation levels following SAK3 (0.1 nM) treatment in the hippocampal CA1 region (SAK3 + NNC 55-0396 1  $\mu\text{M}$ :  $109.8 \pm 3.4$ ,  $p > 0.05$  vs. vehicle,  $p < 0.05$  vs. SAK3; Fig. 1E). Although TTX (100 nM) reduced CaMKII autophosphorylation levels, SAK3 (0.1 nM) still enhanced CaMKII autophosphorylation (SAK3 + TTX:  $139.9 \pm 9.8$ ,  $p < 0.05$  vs. vehicle,  $p < 0.01$  vs. TTX; Fig. 1E). As previous report indicated that T-VGCC blocker mibefradil inhibits basal CaMKII autophosphorylation levels in the mouse striatum (Pasek et al., 2015), we tested whether NNC 55-0396 alone affects CaMKII autophosphorylation levels in the hippocampal slice. NNC 55-0396 (1  $\mu\text{M}$ ) did not alter CaMKII basal autophosphorylation levels ( $103.8 \pm 9.3$ ,  $p > 0.05$  vs. vehicle), whereas high dose (100  $\mu\text{M}$ ) reduced its autophosphorylation ( $66.2 \pm 14.6$ ,  $p < 0.05$  vs. vehicle). Those results suggest that SAK3 enhances CaMKII autophosphorylation via T-VGCCs activation. Thus, we selected SAK3 as a candidate cognitive enhancer.

To further investigate effect of SAK3 on T-VGCC currents, we first carried out whole-cell patch-clamp recording using neuro2A cells transfected with expression vectors harboring cDNAs encoding Cav3.1, 3.2 or 3.3. All three types of T-VGCC currents reached a peak at  $-40$  mV and were completely blocked by

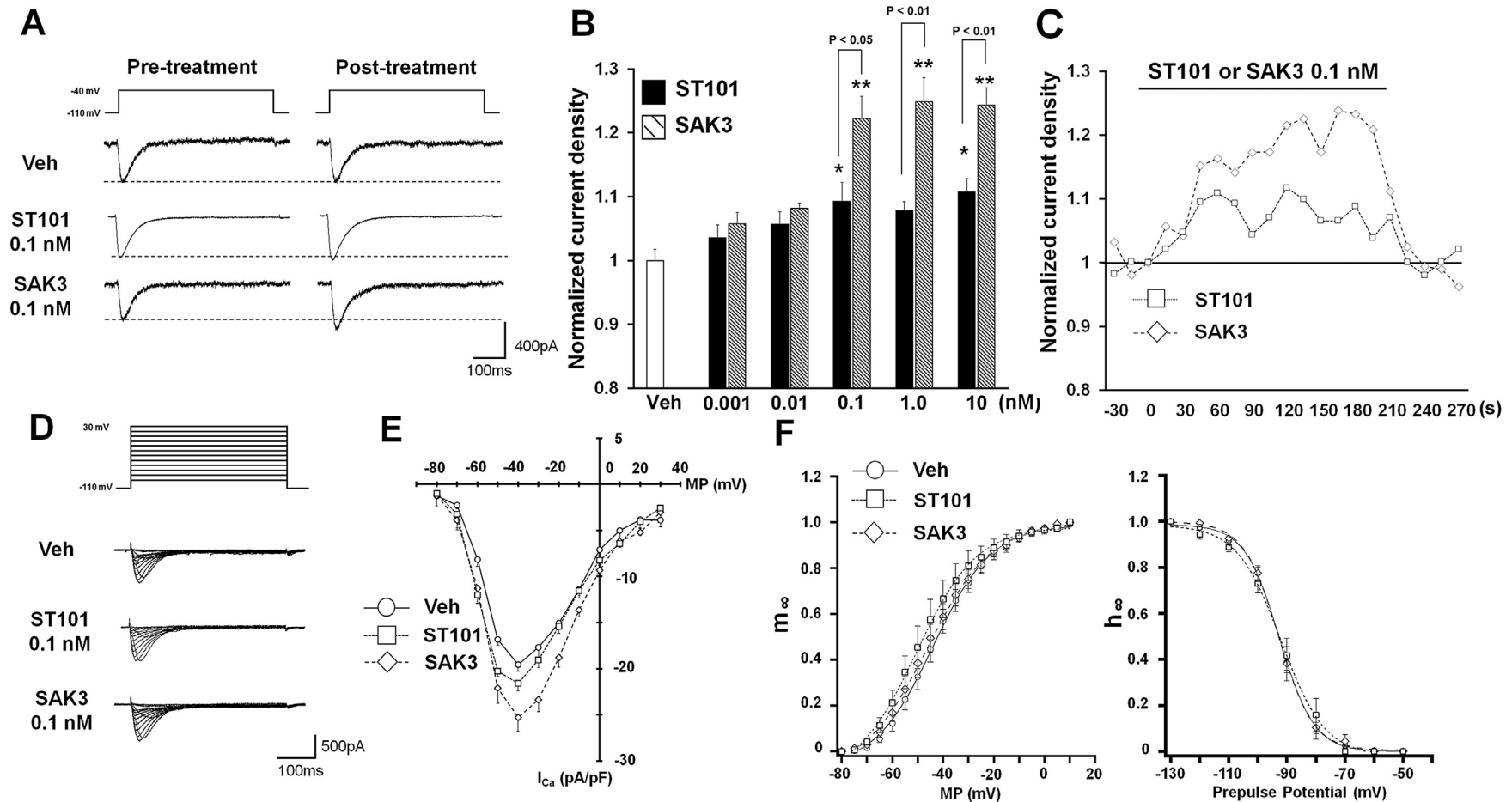


**Fig. 4.** The effect of ST101 and SAK3 on Cav3.3 currents. (A) Representative traces of Cav3.3 peak current following vehicle, ST101 (0.1 nM) or SAK3 (0.1 nM) application. (B) Dose responses following ST101 or SAK3 application were analyzed from 0.001 to 10 nM [SAK3 (0.1 nM) application:  $n = 15$ ; other group:  $n = 5$  per group]. (C) ST101 (0.1 nM) and SAK3 (0.1 nM) application rapidly increased  $Ca^{2+}$  currents in Cav3.3-overexpressing neuro2A cells. (D) Representative voltage-dependent traces of Cav3.3 activity following vehicle, ST101 (0.1 nM) or SAK3 (0.1 nM) application. (E)  $I$ - $V$  relationships following vehicle, ST101 (0.1 nM) or SAK3 (0.1 nM) application (vehicle application:  $n = 9$ ; ST101 application:  $n = 6$ ; SAK3 application:  $n = 9$ ). (F) Steady-state activation (vehicle application:  $n = 7$ ; ST101 application:  $n = 6$ ; SAK3 application:  $n = 7$ ) (left) or inactivation (vehicle application:  $n = 7$ ; ST101 application:  $n = 5$ ; SAK3 application:  $n = 7$ ) (right) curves were not altered by both compounds (0.1 nM) application. (D) Error bars represent SEM.  $*p < 0.05$  vs. vehicle application,  $**p < 0.01$  vs. vehicle application; Veh: vehicle application.

application of NNC 55-0396 (1  $\mu$ M), indicating that cells sufficiently express the transgene (Supplemental Fig. 1). Next, we asked whether ST101 or SAK3 promoted Cav3.1 peak currents. We observed a significant group effect on Cav3.1 currents following drug treatment [ $F(10, 104) = 19.390$ ,  $p < 0.0001$ ]. ST101 (0.001–10 nM), and SAK3 (0.001–10 nM) significantly enhanced Cav3.1 currents compared with vehicle application (ST101; 0.001 nM:  $1.06 \pm 0.0074$ ,  $p < 0.01$  vs. vehicle, 0.01 nM  $1.09 \pm 0.012$ ,  $p < 0.01$  vs. vehicle, 0.1 nM  $1.10 \pm 0.014$ ,  $p < 0.01$  vs. vehicle, 1.0 nM  $1.08 \pm 0.014$ ,  $p < 0.01$  vs. vehicle, 10 nM  $1.07 \pm 0.0095$ ,  $p < 0.01$  vs. vehicle; SAK3; 0.001 nM:  $1.07 \pm 0.0096$ ,  $p < 0.01$  vs. vehicle, 0.01 nM  $1.11 \pm 0.0095$ ,  $p < 0.01$  vs. vehicle, 0.1 nM  $1.20 \pm 0.023$ ,  $p < 0.01$  vs. vehicle, 1.0 nM  $1.18 \pm 0.024$ ,  $p < 0.01$  vs. vehicle, 10 nM  $1.15 \pm 0.015$ ,  $p < 0.01$  vs. vehicle; Fig. 2A and B). Interestingly, SAK3 (0.1–10 nM) application markedly enhanced Cav3.1 currents compared to the same dose of ST101 (Fig. 2A and B). In addition, we observed that both SAK3 and ST101 increased Cav3.1 peak currents immediately after application through a Y-tube (Fig. 2C). Densities of *I*-*V* relationships with SAK3 (0.1 nM) application were significantly larger than those following vehicle or ST101 (0.1 nM) application at several voltages (–50 mV;  $-30.0 \pm 1.99$  pA/pF,  $p < 0.05$  vs. vehicle and  $p > 0.05$  vs. ST101; –40 mV,  $-38.2 \pm 0.83$  pA/pF,  $p < 0.01$  vs. vehicle and  $p < 0.01$  vs. ST101; –30 mV,  $-36.4 \pm 1.19$  pA/pF,  $p < 0.01$  vs. vehicle and  $p < 0.05$  vs. ST101; –20 mV,  $-29.4 \pm 1.46$  pA/pF,  $p < 0.05$  vs. vehicle and  $p > 0.05$  vs. ST101; Fig. 2D and E). We next asked whether SAK3-enhanced Cav3.1 currents were due to changes in steady-state activation and inactivation of Cav3.1 channel. Application of either SAK3 (0.1 nM) or ST101 (0.1 nM) induced no significant change in activation and inactivation curves, indicating that SAK3 promotes Cav3.1 currents without altering channel biophysical properties (Fig. 2F).

### 3.2. SAK3 enhances Cav3.3 but not Cav3.2 currents

As SAK3 was a more powerful activator of Cav3.1 currents than ST101, we evaluated the effect of SAK3 on Cav3.2 and Cav3.3 currents. Neither doses of ST101 (0.001–10 nM) nor SAK3 (0.001–10 nM) enhance Cav3.2 currents (Fig. 3A, B, C). Thus, SAK3 (0.1 nM) application did not promote changes in Cav3.2 peak currents or alter the *I*-*V* relationship (Fig. 3D). On the other hand, Cav3.3 currents significantly increased following ST101 (0.1 nM  $1.11 \pm 0.023$ ,  $p < 0.05$  vs. vehicle, 10 nM  $1.11 \pm 0.021$ ,  $p < 0.05$  vs. vehicle; Fig. 4A and B) and SAK3 application (0.1 nM  $1.22 \pm 0.035$ ,  $p < 0.01$  vs. vehicle; 1.0 nM  $1.25 \pm 0.038$ ,  $p < 0.01$  vs. vehicle, 10 nM  $1.24 \pm 0.027$ ,  $p < 0.01$  vs. vehicle; Fig. 4A and B). SAK3 (0.1–10 nM) application significantly enhanced Cav3.3 currents compared to the same dose of ST101 (Fig. 4A and B). We also confirmed that both ST101 and SAK3 increased Cav3.3 peak currents immediately after application like Cav3.1 currents (Fig. 4C). ST101 (0.1 nM) and SAK3 (0.1 nM) application significantly enhanced densities of *I*-*V* relationships compared with vehicle application, with a peak of –40 mV (ST101: –50 mV  $-20.3 \pm 0.93$  pA/pF,  $p < 0.05$  vs. vehicle; –40 mV,  $-21.6 \pm 0.55$  pA/pF,  $p < 0.05$  vs. vehicle; SAK3: –50 mV;  $-22.1 \pm 1.61$  pA/pF,  $p < 0.05$  vs. vehicle; –40 mV,  $-25.3 \pm 1.46$  pA/pF,  $p < 0.01$  vs. vehicle; –30 mV,  $-23.3 \pm 1.34$  pA/pF,  $p < 0.01$  vs. vehicle; –20 mV,  $-18.8 \pm 1.04$  pA/pF,  $p < 0.05$  vs. vehicle; –10 mV,  $-13.6 \pm 0.74$  pA/pF,  $p < 0.05$  vs. vehicle; Fig. 4D and E). In addition, SAK3 (0.1 nM) significantly increased Cav3.3 currents at several voltages compared with ST101 (–40 mV  $p < 0.05$  vs. ST101, –30 mV  $p < 0.05$  vs. ST101, –20 mV  $p < 0.05$  vs. ST101). Similar to observation in Cav3.1-transfected cells, ST101 (0.1 nM) and SAK3 (0.1 nM) application did not alter channel activation or inactivation properties in Cav3.3-transfected cells (Fig. 4F).

### 3.3. Cav3.1 and 3.3 T-VGCCs are localized to cholinergic nerves in hippocampus and the medial septum

T-VGCCs mRNAs are highly expressed in rodent hippocampus (Talley et al., 1999); however, their precise cellular localization remained unclear. Thus, we assessed localization of Cav3.1 and 3.3 T-VGCCs in mouse brain using antibodies with specificity previously confirmed in rodents (Hildebrand et al., 2009; Liu et al., 2011). Since ST101 enhanced ACh release in mouse hippocampus (Yamaguchi et al., 2006; Yamamoto et al., 2013), we anticipated that T-VGCC would be localized to cholinergic nerves in brain. As expected, Cav3.1 and 3.3 T-VGCCs were expressed in a part of ChAT-positive cholinergic terminals in hippocampal CA1 and CA3 regions (Fig. 5A, B, C, D). Both Cav3.1 and Cav3.3 were also faintly expressed in cell bodies of hippocampal pyramidal neurons, especially in CA3 (Fig. 5A, B, C, D). In addition, we also observed Cav3.1 and Cav3.3 expression in ChAT-positive neurons in the medial septum (Fig. 5E). Although Cav3.1 and 3.3 T-VGCCs are preferentially expressed in the medial septum neurons, it is also detected in the puncta in the hippocampus, in where the immunoreactivity may reflect the presynaptic ChAT and postsynaptic T-VGCCs immunoreactivities. Taken together, this analysis confirms that Cav3.1 and Cav3.3 are expressed in cholinergic neurons.

### 3.4. Acute SAK3 oral administration promotes ACh release in hippocampal CA1 via T-VGCC stimulation

To assess the physiological relevance of Cav3.1 and Cav3.3 localization in cholinergic neurons, we evaluated effect of SAK3 on hippocampal ACh release. A significant group effect on ACh release levels was observed in all treatment groups [ $F(3, 10) = 106.714$ ,  $p < 0.0001$ ]. SAK3 (0.5 mg/kg, p.o.) significantly increased ACh release in CA1, peaking at 20 min after oral administration [The rate of change of ACh for 60 min;  $590.9 \pm 32.7\%$  of control,  $p < 0.01$  vs. vehicle-treated mice and  $p < 0.01$  vs. ST101 (0.5 mg/kg, p.o.)-treated mice; Fig. 6A and B], while acute ST101 (0.5 mg/kg, p.o.) administration did not enhance ACh release (Fig. 6A and B). Importantly, SAK3-induced ACh release was significantly blocked by NNC 55-0396 (1  $\mu$ M) administration through a microdialysis probe [The rate of change of ACh for 60 min;  $196.5 \pm 24.8\%$  of control,  $p < 0.05$  vs. vehicle-treated mice and  $p < 0.01$  vs. SAK3 (0.5 mg/kg, p.o.)-treated mice; Fig. 6A and B]. These observations suggest that SAK3 may promote ACh release via stimulating T-VGCC located in the cholinergic neurons of medial septum and its terminals in the hippocampus. We also evaluated ACh content of hippocampal tissue 30 min after ST101 or SAK3 administration. A significant group effect on ACh levels was observed in all treatment groups in naïve animals [ $F(5, 32) = 12.271$ ,  $p < 0.0001$ ] (Fig. 6C) and in OBX animals [ $F(4, 28) = 8.707$ ,  $p = 0.0001$ ] (Fig. 6D). SAK3 administration (at 0.5 or 1.0 mg/kg, p.o.) significantly elevated ACh levels in the CA1 region (0.5 mg/kg;  $403.1 \pm 26.2$  fmol/mg,  $p < 0.01$  vs. vehicle-treated mice; 1.0 mg/kg;  $467.7 \pm 48.3$  fmol/mg,  $p < 0.01$  vs. vehicle-treated mice; Fig. 6C), whereas acute ST101 (0.5 mg/kg, p.o.) administration did not enhance ACh levels. In addition, reduced ACh levels seen in the hippocampal CA1 region of OBX mice were rescued by acute SAK3 (0.5 mg/kg, p.o.), but not ST101 (0.5 mg/kg, p.o.) administration [OBX mice with vehicle administration;  $141.8 \pm 48.3$  fmol/mg,  $p < 0.05$  vs. vehicle-treated mice; OBX mice with SAK3 (0.5 mg/kg, p.o.) administration;  $271.1 \pm 33.5$  fmol/mg,  $p > 0.05$  vs. vehicle-treated mice and  $p < 0.01$  vs. vehicle-treated OBX mice; Fig. 6D]. SAK3 effects on ACh levels in CA1 of naïve and OBX mice were totally blocked by NNC 55-0396 (12.5 mg/kg, i.p.) treatment initiated 30 min before SAK3 administration [naïve mice;  $190.1 \pm 14.9$  fmol/mg,  $p > 0.05$  vs. vehicle-treated mice and  $p < 0.01$  vs. SAK3 (0.5 mg/kg, p.o.)-treated mice;

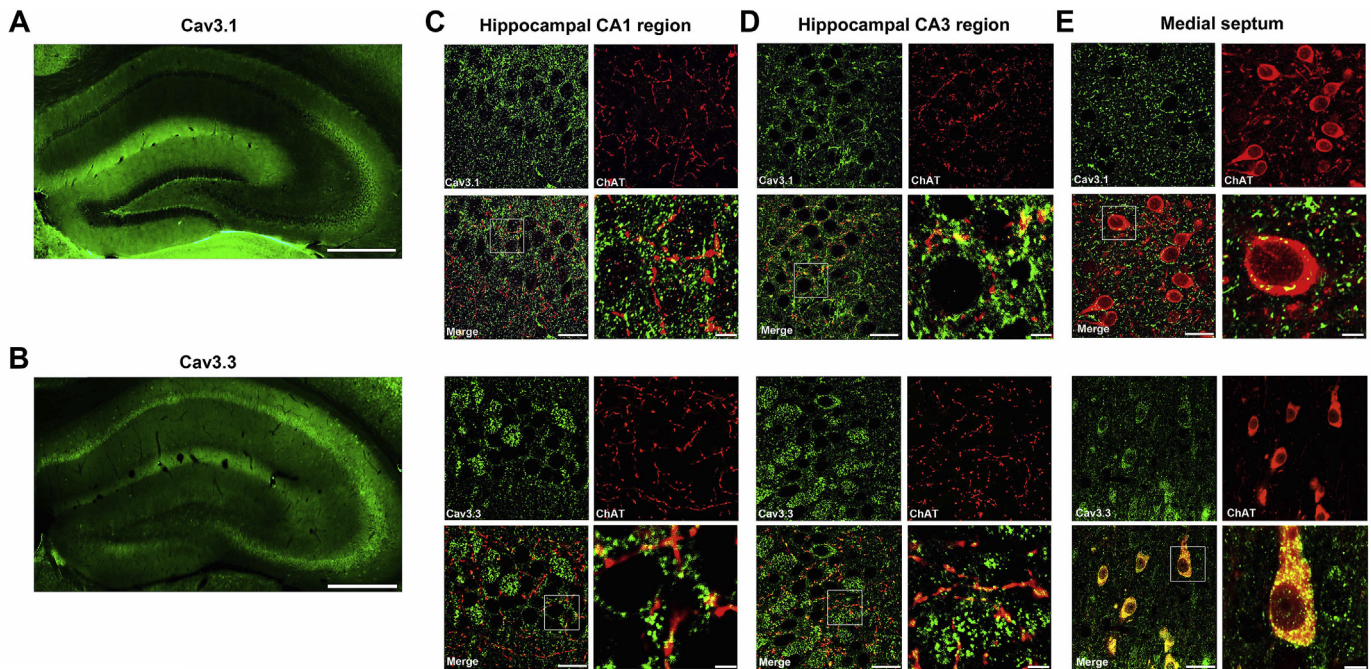


**Fig. 5.** Cav3.1 and 3.3 T-VGCCs are localized to cholinergic neurons. Immunohistochemical studies of Cav3.1 and 3.3 were performed in mouse hippocampus and septum. (A) Cav3.1 T-VGCCs (green) are expressed over the entire hippocampus. Scale bar: 100  $\mu$ m. (B) Representative expression pattern of Cav3.3 T-VGCCs (green) in hippocampus. Scale bar: 100  $\mu$ m. (C, D, E) Confocal images showing Cav3.1 (green, upper), Cav3.3 (green, bottom) and ChAT (red) colocalization in hippocampal CA1 (C) and CA3 (D) regions and in the medial septum (E). Boxed regions in merged images are shown at higher magnification at immediate right. Scale bars: low magnification, 20  $\mu$ m; high magnification, 5  $\mu$ m.

OBX mice;  $132.9 \pm 12.5$  fmol/mg,  $p < 0.05$  vs. vehicle-treated mice,  $p > 0.05$  vs. vehicle-treated OBX mice and  $p < 0.01$  vs. SAK3 (0.5 mg/kg, p.o.)-treated OBX mice: Fig. 6C and D]. NNC 55-0396 (1  $\mu$ M or 12.5 mg/kg, i.p.) treatment did not affect basal ACh levels in the hippocampus (Supplemental Figs. 2A, B, C). These results suggest that enhancement of T-VGCCs rescues cholinergic nerve activity and SAK3 may be more potent than ST101 as a cognitive enhancer.

Next, we evaluated the effect of SAK3 on ACh levels in Cav3.1 KO mice. Although SAK3-promoted ACh releases were partially inhibited in Cav3.1 KO mice as compared to wild type (WT) mice [The rate of change of ACh for 60 min;  $204.1 \pm 23.4\%$  of control,  $p < 0.05$  vs. vehicle-treated WT mice and  $p < 0.01$  vs. SAK3 (0.5 mg/kg, p.o.)-treated WT mice: Fig. 6E and F], NNC 55-0396 (1  $\mu$ M) completely blocked SAK3-evoked ACh release in Cav3.1 KO mice [The rate of change of ACh for 60 min;  $110.6 \pm 16.8\%$  of control,  $p > 0.05$  vs. vehicle-treated WT mice and  $p < 0.05$  vs. SAK3 (0.5 mg/kg, p.o.)-treated Cav3.1 KO mice: Fig. 6E and F]. In addition, the effect of SAK3 (0.5 mg/kg, p.o.) on ACh contents of the hippocampal CA1 region were significantly blocked in Cav3.1 KO mice with or without NNC 55-0396 (12.5 mg/kg, i.p.) [Cav3.1 KO mice with SAK3 (0.5 mg/kg, p.o.) administration;  $497.9 \pm 27.5$  fmol/mg,  $p > 0.05$  vs. vehicle-treated WT mice,  $p < 0.01$  vs. SAK3-treated WT mice; Cav3.1 KO mice with SAK3 (0.5 mg/kg, p.o.) administration following NNC 55-0396 (12.5 mg/kg, i.p.) treatment;  $342.6 \pm 42.1$  fmol/mg,  $p > 0.05$  vs. vehicle-treated WT mice and  $p > 0.05$  vs. SAK3-treated Cav3.1 KO mice: Fig. 6G]. These results supported that SAK3 activates cholinergic nerve activities via enhancing T-VGCCs and that Cav3.1 is predominantly involved in the SAK3 enhanced ACh release in the hippocampus.

### 3.5. Acute SAK3 administration rescues impaired memory-related behaviors in OBX mice

To confirm the relevance of enhanced ACh release to cognition, we asked whether acute SAK3 improves memory deficits observed

in OBX mice. We observed a significant group effect in all treatment groups in terms of spontaneous alternation behavior in a Y-maze task [ $F(8, 45) = 4.594$ ,  $p = 0.0004$ ] and retention time in a passive avoidance task [ $F(8, 45) = 21.760$ ,  $p < 0.0001$ ]. Oral administration of SAK3 (0.5 or 1.0 mg/kg, p.o.) improved decreased alternation behaviors observed in OBX mice (0.5 mg/kg;  $73.7 \pm 3.9\%$ ,  $p > 0.05$  vs. vehicle-treated mice and  $p < 0.01$  vs. vehicle-treated OBX mice; 1.0 mg/kg;  $73.5 \pm 4.7\%$ ,  $p > 0.05$  vs. vehicle-treated mice and  $p < 0.01$  vs. vehicle-treated OBX mice: Fig. 7A). Acute SAK3 (0.5 or 1.0 mg/kg, p.o.) administration also rescued reduced retention time in the passive avoidance task (0.5 mg/kg;  $168.9 \pm 58.8$  s,  $p < 0.01$  vs. vehicle-treated mice and  $p < 0.01$  vs. vehicle-treated OBX mice; 1.0 mg/kg;  $183.3 \pm 53.5$  s,  $p < 0.05$  vs. vehicle-treated mice and  $p < 0.01$  vs. vehicle-treated OBX mice: Fig. 7B). Moreover, acute SAK3 (0.5 or 1.0 mg/kg, p.o.) administration restored the ability to discriminate familiar from novel objects without altering the discrimination index in the trial session (Fig. 7C). Importantly, pre-administration of NNC 55-0396 (12.5 mg/kg, i.p.) totally blocked behavioral improvements elicited by acute SAK3 (0.5 mg/kg, p.o.) administration (alternation in the Y-maze task;  $54.7 \pm 3.5\%$ ,  $p = 0.096$  vs. vehicle-treated mice,  $p > 0.05$  vs. vehicle-treated OBX mice and  $p < 0.05$  vs. vehicle-treated OBX mice: Fig. 7). On the other hand, acute ST101 (0.5 mg/kg, p.o.) administration did not rescue impaired memory or cognition in OBX mice (Fig. 7), indicating overall that SAK3 has a more potent effect on memory than does ST101. NNC 55-0396 (12.5 mg/kg, i.p.) treatment alone did not affect all memory-related behaviors (Supplemental Figs. 2D, E, F).

## 4. Discussion

In the present study, we found that SAK3 is superior to ST101 in facilitation of Cav3.1 and Cav3.3 currents. We also report the following novel observations: 1) SAK3 increased T-VGCC currents without altering channel activation and inactivation properties; 2) Cav3.1 and Cav3.3 T-VGCCs were localized to septo-hippocampal

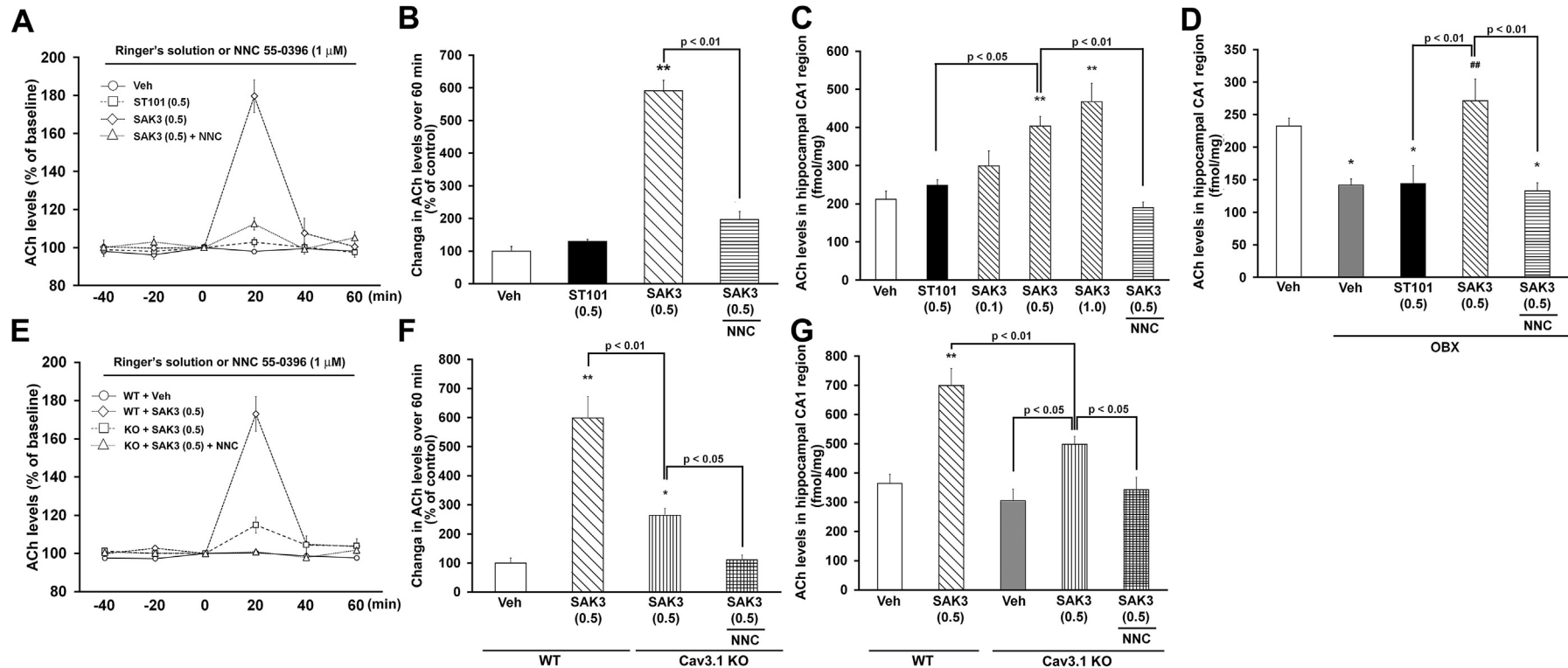


**Fig. 6.** SAK3 promotes ACh release in hippocampal CA1 via T-VGCC stimulation. (A) Time zero defines the point immediately following oral drug administration. ACh levels in dialysates were measured every 20 min ( $n = 5$  per group). (B) SAK3 (0.5 mg/kg, p.o.) administration enhanced ACh levels via T-VGCC activation ( $n = 5$  per group). Error bars represent SEM. \*\* $p < 0.01$  vs. vehicle-treated naïve mice. (C) ACh content in hippocampal CA1 in naïve mice ( $n = 6-7$  per group). Error bars represent SEM. \* $p < 0.05$  vs. vehicle-treated naïve mice; \*\* $p < 0.01$  vs. vehicle-treated naïve mice. (D) Acute SAK3 (0.5 mg/kg, p.o.) administration rescued reduced ACh levels seen in OBX mice ( $n = 6-7$  per group). Error bars represent SEM. \* $p < 0.05$  vs. vehicle-treated control mice. (E) Time zero defines the point immediately after oral drug administration. ACh levels in dialysates were measured every 20 min in C57BL6 WT and Cav3.1 KO mice ( $n = 5$  per group). (F) The effect of SAK3 (0.5 mg/kg, p.o.) on ACh release in WT and Cav3.1 KO mice with or without T-VGCC blocker ( $n = 5$  per group). Error bars represent SEM. \* $p < 0.05$  vs. vehicle-treated WT mice, \*\* $p < 0.01$  vs. vehicle-treated WT mice. (G) Acute SAK3 (0.5 mg/kg, p.o.) administration failed to enhance ACh levels in hippocampal CA1 in Cav3.1 KO mice with or without T-VGCC blocker ( $n = 5-6$  per group). Error bars represent SEM. \* $p < 0.05$  vs. vehicle-treated control mice. Veh: vehicle treatment, ST101: oral ST101 administration, SAK3: oral SAK3 administration, NNC: NNC 55-0396 (12.5 mg/kg, i.p.) intraperitoneal injection, OBX: olfactory-bulbectomized.

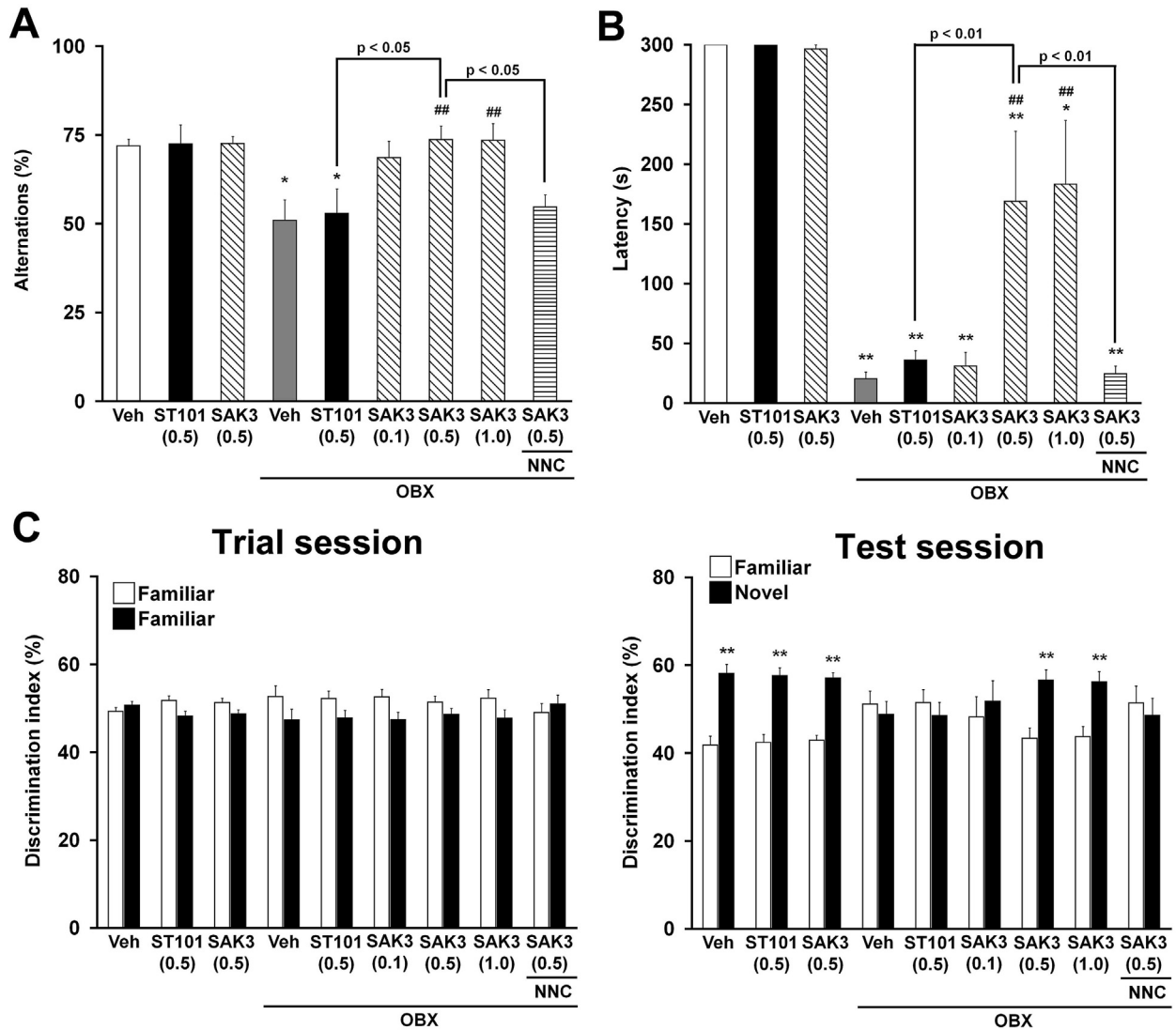


**Fig. 7.** Acute SAK3 administration rescues impaired memory-related behaviors in OBX mice via T-VGCC activation. (A) Alternations in a Y-maze task were measured at 2 weeks after bulbectomy. Decreased alternation behaviors in OBX mice were rescued by acute SAK3 (0.5 or 1.0 mg/kg, p.o.) administration, and the SAK3 effect (at 0.5 mg/kg, p.o.) was blocked following NNC 55-0396 (12.5 mg/kg, i.p.) treatment (n = 6 per group). Error bars represent SEM. \*p < 0.05 vs. vehicle-treated control mice; ##p < 0.01 vs. vehicle-treated OBX mice. (B) Acute SAK3 (0.5 and 1.0 mg/kg, p.o.) administration improved shortened latency time on retention trials in OBX mice (n = 6 per group). Error bars represent SEM. \*p < 0.05; \*\*p < 0.01 vs. vehicle-treated control mice; ##p < 0.01 vs. vehicle-treated OBX mice. (C) No differences were observed in the trial session between groups (n = 6 per group). The impaired discrimination index in OBX mice was improved by acute oral administration of SAK3 (0.5 mg/kg, p.o.) but not ST101 (0.5 mg/kg, p.o.) (n = 6 per group). Error bars represent SEM. \*\*p < 0.01 vs. the familiar group.

cholinergic neurons, where they enhanced ACh release; and 3) acute SAK3 but not ST101 acute administration improved memory impairment seen in OBX mice via T-VGCC stimulation.

T-VGCC voltage sensors are located in segment 4 of each of the four repeated domains, and synchronous activation of all sensors is required for channel opening (Perez-Reyes, 2003). However, SAK3 (0.1 nM) treatment did not alter steady-state activation or inactivation of Cav3.1 or Cav3.3, indicating that it does not interact with T-VGCC voltage sensors. On the other hand, T-VGCC activities are also mediated by intracellular factors such as protein kinase A (PKA), protein kinase C (PKC), CaMKII, or Gβγ protein (Chemin et al., 2007; Iftinca et al., 2007; Lu et al., 1994; Tao et al., 2008; Zhang et al., 2013). In particular, PKA and PKC promote all three T-VGCC currents by phosphorylating serine/threonine residues in the intracellular II-III loop (Chemin et al., 2007; Zhang et al., 2013). Treatment with membrane-permeable cAMP analogues or PKC agonists for 10 min stimulates all human T-VGCC currents at 37 °C

but not at room temperature (Chemin et al., 2007). Protein kinase-mediated T-VGCC currents normally evoke a peak response by 15–60 min after agonist treatment (Chemin et al., 2007; Iftinca et al., 2007). Here, T-VGCC currents were measured at room temperature, and SAK3-promoted currents plateaued within 3 min of drug application (Figs. 2C and 3B), suggesting that SAK3 may directly enhance Cav3.1 and Cav3.3 currents independent of intracellular signaling. As channel current is determined by the number of functional channels, the probability of channel opening and single channel conductance (Tsien et al., 1986; Hille, 2001), SAK3 may influence single channel properties. Further studies are required to define the mechanism underlying the effects of SAK3 on T-VGCCs.

Previous studies indicate that T-VGCCs are located in GABAergic neurons, and that T-VGCC inhibitors prevent ACh- or dopamine-evoked GABA release in rodent hippocampus and cerebral cortex (Liu et al., 2011; Tang et al., 2011; Cilz et al., 2014). In spinal neurons,

low doses of  $\text{Ni}^{2+}$  and mibefradil attenuate spontaneous excitatory postsynaptic currents (Bao et al., 1998), suggesting that T-VGCCs function in neurotransmission consist of a low-threshold component of fast exocytosis (Carbone et al., 2006; Cueni et al., 2009). Here, we used specific antibodies to detect Cav3.1 and 3.3 localization in mouse cholinergic neurons. We did not detect Cav3.1 and 3.3 immunoreactivity in GAD-positive GABAergic terminals in mouse hippocampus (data not shown). In agreement, *in situ* hybridization shows that rat cholinergic neurons in the medial septum express Cav3.1 and 3.3 mRNA (Talley et al., 1999), and T-VGCC currents are observed in the isolated septal neurons (Griffith et al., 1994; Perez-Reyes, 2003), suggesting that Cav3.1 and 3.3 T-VGCCs participate in cholinergic neuronal activity. A previous study indicated that the T-VGCC blocker zonisamide (5 mM) inhibits basal and high  $\text{K}^{+}$ -induced ACh release in rat frontal cortex (Zhu et al., 2002). In our study, NNC 55-0396 (1  $\mu\text{M}$ ) blocked SAK3-promoted ACh release without altering basal ACh levels, whereas we observed that NNC 55-0396 (100  $\mu\text{M}$ ) application via a microdialysis probe significantly decreased basal ACh release (Supplemental Figs. 2A and B). Moreover, SAK3 (0.5 mg/kg, p.o.)-induced ACh levels in the hippocampus largely attenuated in Cav3.1 KO mice (Fig. 6). It had been reported that chronic ST101 (0.01, 0.1 or 1.0 mg/kg, p.o.) treatment restores reduced ChAT activity by unknown mechanism in the medial septum and hippocampus of amyloid- $\beta$  infused rats (Yamaguchi et al., 2006). In the present study, acute SAK3 administration could increase ACh contents in the hippocampal CA1 region in both naïve and OBX mice via T-VGCCs (Fig. 6C, D, G). Acute SAK3 administration may also increase ChAT activity in the hippocampus. Taken together, T-VGCCs play an important role in cholinergic neuronal activity, including ACh release in brain.

Cholinergic pathways are critical for learning and memory processes (Melancon et al., 2013; Pandya and Yakel, 2013), and reduced cholinergic nerve activity is closely associated with cognitive decline in neurodegenerative diseases such as AD and dementia with Lewy body (Mukaetova-Ladinska et al., 2013; Paul et al., 2015). Thus, acute SAK3 administration likely improves cognitive impairment seen in OBX mice by increasing ACh release following hippocampal T-VGCC enhancement. On the other hand, T-VGCCs are expressed in both cortical and hippocampal pyramidal neurons (Takahashi and Akaike, 1991; Perez-Reyes, 2003; McKay et al., 2006), thereby contributing to NMDA receptor-dependent LTP (Thomas et al., 1998; Kampa et al., 2006; Cueni et al., 2009). In addition, T-VGCC blockers decrease CaMKII activity, which is essential for learning and memory acquisition (Fukunaga et al., 2009; Pasek et al., 2015). We previously reported that incubation of acute cortical slices with ST101 (0.1 nM) stimulates T-VGCCs and promotes LTP induction and maintenance via CaMKII activation (Moriguchi et al., 2012). Moreover, SAK3 (0.1 nM) treatment enhances CaMKII activity in hippocampal CA1 slices via T-VGCC enhancement (Fig. 1). Thus, SAK3 may enhance neuronal activities in hippocampus either directly or indirectly through glutamatergic pathways.

We previously observed that acute intraperitoneal administration of ST101 significantly improved memory deficits seen in OBX mice (Yamamoto et al., 2013); however, in the present study, acute administration of ST101 via an oral route did not have a comparable effect. Here, ST101 is less potent than SAK3 in T-VGCC activation (Fig. 2). In fact, a single oral administration of ST101 did not rescue impaired spatial memory in OBX mice in a previous study (Shioda et al., 2010). Moreover, ST101 mono-therapy was not sufficient to ameliorate symptoms in AD patients in a phase 2 clinical trial in the USA (Gauthier et al., 2015). Our findings indicate that SAK3 has a more powerful effect on T-VGCC activation and ACh release than does ST101, resulting in improving memory deficits after acute oral administration.

In conclusion, the present study indicates success in developing the novel T-VGCC enhancer SAK3, which is superior to ST101 in terms of enhancing cognition. Moreover, we defined T-VGCC localization and function in cholinergic neurons. These findings suggest that T-VGCCs are novel molecular targets to develop AD therapeutics and that a T-VGCC enhancer such as SAK3 may become a new drug to treat dementia in neurodegenerative disease.

### Disclosure/conflict of interest

The authors have no conflict of interest.

### Acknowledgments

ST101 was gifted by Sonexa Therapeutics Inc. (San Diego, CA, USA). This work was supported in part by grants-in-aid for Scientific Research from the Ministry of Education, Science, Sports and Culture of Japan (Kakenhi 25293124 to K.F.), Project of Translational and Clinical Research Core Centers from Japan Agency for Medical Research and Development (AMED) (B11 to K.F.) and Research Fellow of the Japan Society for the Promotion of Science (266540 to Y.Y.).

### Appendix A. Supplementary data

Supplementary data related to this article can be found at <http://dx.doi.org/10.1016/j.neuropharm.2017.01.011>.

### References

- Abe, T., Takehi, A., Suga, H., Okumura, Y., Itoh, K., 2010. Synthesis of spiro[2-cyclopentene-1,3'-imidazo[1,2a]pyridine] derivatives and their interesting behavior in 1H-NMR spectra in deuteriochloroform. *Heterocycles* 81 (9), 2075–2086.
- Bao, J., Li, J.J., Perl, E.R., 1998. Differences in  $\text{Ca}^{2+}$  channels governing generation of miniature and evoked excitatory synaptic currents in spinal laminae I and II. *J. Neurosci.* 18 (21), 8740–8750.
- Bertrand, N., Beley, P., Beley, A., 1994. Brain fixation for acetylcholine measurements. *J. Neurosci. Methods* 53 (1), 81–85.
- Carbone, E., Giampiccoli, A., Marcantoni, A., Guido, D., Carabelli, V., 2006. A new role for T-type channels in fast “low-threshold” exocytosis. *Cell Calcium* 40 (2), 147–154.
- Chemin, J., Mezghrani, A., Bidaud, I., Dupasquier, S., Marger, F., Barrère, C., Nargeot, J., Lory, P., 2007. Temperature-dependent modulation of  $\text{CaV}3$  T-type calcium channels by protein kinases C and A in mammalian cells. *J. Biol. Chem.* 282 (45), 32710–32718.
- Cilz, N.I., Kurada, L., Hu, B., Lei, S., 2014. Dopaminergic modulation of GABAergic transmission in the entorhinal cortex: concerted roles of  $\alpha 1$  adrenoreceptors, inward rectifier  $\text{K}^{+}$ , and T-type  $\text{Ca}^{2+}$  channels. *Cereb. Cortex* 24 (12), 3195–3208.
- Crunelli, V., Cope, D.W., Hughes, S.W., 2006. Thalamic T-type  $\text{Ca}^{2+}$  channels and NREM sleep. *Cell Calcium* 40, 175–190.
- Cueni, L., Canepari, M., Adelman, J.P., Lüthi, A., 2009.  $\text{Ca}^{2+}$  signaling by T-type  $\text{Ca}^{2+}$  channels in neurons. *Pflugers Arch.* 457 (5), 1161–1172.
- François, A., Laffray, S., Pizzoccaro, A., Eschalier, A., Bourinet, E., 2014. T-type calcium channels in chronic pain: mouse models and specific blockers. *Pflugers Arch.* 466 (4), 707–717.
- Fukunaga, K., Goto, S., Miyamoto, E., 1988. Immunohistochemical localization of  $\text{Ca}^{2+}$ /calmodulin-dependent protein kinase II in rat brain and various tissues. *J. Neurochem.* 51, 1070–1078.
- Fukunaga, K., Shioda, N., Miyamoto, E., 2009. The function of CaM kinase II in synaptic plasticity and spine formation. In: Lajtha, A. (Ed.), *Handbook of Neurochemistry and Molecular Neurobiology Neural Signaling Mechanisms*. Springer, New York, pp. 163–183.
- Gauthier, S., Rountree, S., Finn, B., LaPlante, B., Weber, E., Oltersdorf, T., 2015. Effects of the acetylcholine release agent ST101 with donepezil in Alzheimer's disease: a randomized phase 2 study. *J. Alzheimers Dis.* 48 (2), 473–481.
- Griffith, W.H., Taylor, L., Davis, M.J., 1994. Whole-cell and single-channel calcium currents in Guinea pig basal forebrain neurons. *J. Neurophysiol.* 71 (6), 2359–2376.
- Green, K.N., Khashwji, H., Estrada, T., Laferla, F.M., 2011. ST101 induces a novel 17 kDa APP cleavage that precludes  $\text{A}\beta$  generation in vivo. *Ann. Neurol.* 69 (5), 831–844.
- Handforth, A., Homanics, G.E., Covey, D.F., Krishnan, K., Lee, J.Y., Sakimura, K.,

- Martin, F.C., Quesada, A., 2010. T-type calcium channel antagonists suppress tremor in two mouse models of essential tremor. *Neuropharmacology* 59 (6), 380–387.
- Han, F., Shioda, N., Moriguchi, S., Yamamoto, Y., Raie, A.Y., Yamaguchi, Y., Hino, M., Fukunaga, K., 2008. Spiro[imidazo[1,2-a]pyridine-3,2-indan]-2(3H)-one (ZSET1446/ST101) treatment rescues olfactory bulbectomy-induced memory impairment by activating Ca<sup>2+</sup>/calmodulin kinase II and protein kinase C in mouse hippocampus. *J. Pharmacol. Exp. Ther.* 326, 127–134.
- Hildebrand, M.E., Isope, P., Miyazaki, T., Nakaya, T., Garcia, E., Feltz, A., Schneider, T., Hescheler, J., Kano, M., Sakimura, K., Watanabe, M., Dieudonné, S., Snutch, T.P., 2009. Functional coupling between mGluR1 and Cav3.1 T-type calcium channels contributes to parallel fiber-induced fast calcium signaling within Purkinje cell dendritic spines. *J. Neurosci.* 29 (31), 9668–9682.
- Hille, B., 2001. *Ion Channels of Excitable Membranes*, third ed. Sinauer Associates, Inc, Sunderland, Massachusetts, U.S.A.
- Huguenard, J.R., 1996. Low-threshold calcium currents in central nervous system neurons. *Annu. Rev. Physiol.* 58, 329–348.
- Iftinca, M., Hamid, J., Chen, L., Varela, D., Tadayonnejad, R., Altier, C., Turner, R.W., Zamponi, G.W., 2007. Regulation of T-type calcium channels by Rho-associated kinase. *Nat. Neurosci.* 10 (7), 854–860.
- Kampa, B.M., Letzkus, J.J., Stuart, G.J., 2006. Requirement of dendritic calcium spikes for induction of spike-timing-dependent synaptic plasticity. *J. Physiol.* 574 (Pt 1), 283–290.
- Kato, K., Wakamori, M., Mori, Y., Imoto, K., Kitamura, K., 2002. Inhibitory effects of cilnidipine on peripheral and brain N-type Ca<sup>2+</sup> channels expressed in BHK cells. *Neuropharmacology* 42 (8), 1099–1108.
- Lee, S., Ahmed, T., Lee, S., Kim, H., Choi, S., Kim, D.S., Kim, S.J., Cho, J., Shin, H.S., 2011. Bidirectional modulation of fear extinction by mediadorsal thalamic firing in mice. *Nat. Neurosci.* 15 (2), 308–314.
- Liu, X.B., Murray, K.D., Jones, E.G., 2011. Low-threshold calcium channel subunit Ca<sub>v</sub>(v) 3.3 is specifically localized in GABAergic neurons of rodent thalamus and cerebral cortex. *J. Comp. Neurol.* 519 (6), 1181–1195.
- Lu, H.K., Fern, R.J., Nee, J.J., Barrett, P.Q., 1994. Ca<sup>2+</sup>-dependent activation of T-type Ca<sup>2+</sup> channels by calmodulin-dependent protein kinase II. *Am. J. Physiol.* 267 (1 Pt 2), F183–F189.
- McCormick, D.A., Bal, T., 1997. Sleep and arousal: thalamocortical mechanisms. *Annu. Rev. Neurosci.* 20, 185–215.
- McKay, B.E., McRory, J.E., Molineux, M.L., Hamid, J., Snutch, T.P., Zamponi, G.W., Turner, R.W., 2006. Ca<sub>v</sub>(V)3 T-type calcium channel isoforms differentially distribute to somatic and dendritic compartments in rat central neurons. *Eur. J. Neurosci.* 24 (9), 2581–2594.
- Melancon, B.J., Tarr, J.C., Panarese, J.D., Wood, M.R., Lindsley, C.W., 2013. Allosteric modulation of the M1 muscarinic acetylcholine receptor: improving cognition and a potential treatment for schizophrenia and Alzheimer's disease. *Drug Discov. Today* 18 (23–24), 1185–1199.
- Miyamoto, Y., Fukuda, T., 2015. Immunohistochemical study on the neuronal diversity and three-dimensional organization of the mouse entopeduncular nucleus. *Neurosci. Res.* 94, 37–49.
- Moriguchi, S., Shioda, N., Yamamoto, Y., Tagashira, H., Fukunaga, K., 2012. The T-type voltage-gated calcium channel as a molecular target of the novel cognitive enhancer ST101: enhancement of long-term potentiation and CaMKII autophosphorylation in rat cortical slices. *J. Neurochem.* 121, 44–53.
- Mukaetova-Ladinska, E.B., Andras, A., Milne, J., Abdel-All, Z., Borr, I., Jaros, E., Perry, R.H., Honer, W.G., Cleghorn, A., Doherty, J., McIntosh, G., Perry, E.K., Kalaria, R.N., McKeith, I.G., 2013. Synaptic proteins and choline acetyltransferase loss in visual cortex in dementia with Lewy bodies. *J. Neuropathol. Exp. Neurol.* 72 (1), 53–60.
- Nevejan, T., Sakmann, B., 2006. Spine Ca<sup>2+</sup> signaling in spike-timing-dependent plasticity. *J. Neurosci.* 26 (43), 11001–11013.
- Pandya, A.A., Yakel, J.L., 2013. Effects of neuronal nicotinic acetylcholine receptor allosteric modulators in animal behavior studies. *Biochem. Pharmacol.* 86 (8), 1054–1062.
- Pasek, J.G., Wang, X., Colbran, R.J., 2015. Differential CaMKII regulation by voltage-gated calcium channels in the striatum. *Mol. Cell Neurosci.* 68, 234–243.
- Paul, S., Jeon, W.K., Bizoz, J.L., Han, J.S., 2015. Interaction of basal forebrain cholinergic neurons with the glucocorticoid system in stress regulation and cognitive impairment. *Front. Aging Neurosci.* 7, 43.
- Paxinos, G., Franklin, K.B.J., 2001. *The Mouse Brain in Stereotaxic Coordinates*. Academic, San Diego.
- Perez-Reyes, E., 2003. Molecular physiology of low-voltage-activated t-type calcium channels. *Physiol. Rev.* 83 (1), 117–161.
- Schmidt-Hieber, C., Jonas, P., Bischofberger, J., 2004. Enhanced synaptic plasticity in newly generated granule cells of the adult hippocampus. *Nature* 429 (6988), 184–187.
- Shioda, N., Yamamoto, Y., Han, F., Moriguchi, S., Yamaguchi, Y., Hino, M., Fukunaga, K., 2010. A novel cognitive enhancer, ZSET1446/ST101, promotes hippocampal neurogenesis and ameliorates depressive behavior in olfactory bulbectomized mice. *J. Pharmacol. Exp. Ther.* 333 (1), 43–50.
- Takahashi, K., Akaike, N., 1991. Calcium antagonist effects on low-threshold (T-type) calcium current in rat isolated hippocampal CA1 pyramidal neurons. *J. Pharmacol. Exp. Ther.* 256 (1), 169–175.
- Talley, E.M., Cribbs, L.L., Lee, J.H., Daud, A., Perez-Reyes, E., Bayliss, D.A., 1999. Differential distribution of three members of a gene family encoding low voltage-activated (T-type) calcium channels. *J. Neurosci.* 19 (6), 1895–1911.
- Tang, A.H., Karson, M.A., Nagode, D.A., McIntosh, J.M., Uebele, V.N., Renger, J.J., Klugmann, M., Milner, T.A., Alger, B.E., 2011. Nerve terminal nicotinic acetylcholine receptors initiate quantal GABA release from perisomatic interneurons by activating axonal T-type (Cav3) Ca<sup>2+</sup> channels and Ca<sup>2+</sup> release from stores. *J. Neurosci.* 31 (38), 13546–13561.
- Tao, J., Hildebrand, M.E., Liao, P., Liang, M.C., Tan, G., Li, S., Snutch, T.P., Soong, T.W., 2008. Activation of corticotropin-releasing factor receptor 1 selectively inhibits Cav3.2 T-type calcium channels. *Mol. Pharmacol.* 73 (6), 1596–1609.
- Thomas, M.J., Watabe, A.M., Moody, T.D., Makhinson, M., O'Dell, T.J., 1998. Post-synaptic complex spike bursting enables the induction of LTP by theta frequency synaptic stimulation. *J. Neurosci.* 18 (18), 7118–7126.
- Tsien, R.W., Bean, B.P., Hess, P., Lansman, J.B., Nilius, B., Nowicky, M.C., 1986. Mechanisms of calcium channel modulation by beta-adrenergic agents and dihydropyridine calcium agonists. *J. Mol. Cell Cardiol.* 18 (7), 691–710.
- Wakamori, M., Hidaka, H., Akaike, N., 1993. Hyperpolarizing muscarinic responses of freshly dissociated rat hippocampal CA1 neurones. *J. Physiol.* 463, 585–604.
- Yabuki, Y., Fukunaga, K., 2013. Oral administration of glutathione improves memory deficits following transient brain ischemia by reducing brain oxidative stress. *Neuroscience* 250, 394–407.
- Yabuki, Y., Ohizumi, Y., Yokosuka, A., Mimaki, Y., Fukunaga, K., 2014. Nobiletin treatment improves motor and cognitive deficits seen in MPTP-induced Parkinson model mice. *Neuroscience* 259, 126–141.
- Yabuki, Y., Shinoda, Y., Izumi, H., Ikuno, T., Shioda, N., Fukunaga, K., 2015. Dehydroepiandrosterone administration improves memory deficits following transient brain ischemia through sigma-1 receptor stimulation. *Brain Res.* 1622, 102–113.
- Yamaguchi, Y., Miyashita, H., Tsunekawa, H., Mouri, A., Kim, H.C., Saito, K., Matsuno, T., Kawashima, S., Nabeshima, T., 2006. Effects of a novel cognitive enhancer, spiro[imidazo-[1,2-a]pyridine-3,2-indan]-2(3H)-one (ZSET1446), on learning impairments induced by amyloid-beta1-40 in the rat. *J. Pharmacol. Exp. Ther.* 317 (3), 1079–1087.
- Yamamoto, Y., Shioda, N., Han, F., Moriguchi, S., Fukunaga, K., 2013. Novel cognitive enhancer ST101 enhances acetylcholine release in mouse dorsal hippocampus through T-type voltage-gated calcium channel stimulation. *J. Pharmacol. Sci.* 121, 212–226.
- Zamponi, G.W., Lory, P., Perez-Reyes, E., 2010. Role of voltage-gated calcium channels in epilepsy. *Pflügers Arch.* 460 (2), 395–403.
- Zhang, Y., Jiang, X., Snutch, T.P., Tao, J., 2013. Modulation of low-voltage-activated T-type Ca<sup>2+</sup> channels. *Biochim. Biophys. Acta* 1828 (7), 1550–1559.
- Zhu, G., Okada, M., Murakami, T., Kawata, Y., Kamata, A., Kaneko, S., 2002. Interaction between carbamazepine, zonisamide and voltage-sensitive Ca<sup>2+</sup> channel on acetylcholine release in rat frontal cortex. *Epilepsy Res.* 49 (1), 49–60.